



HAL
open science

DESIGN, SYNTHESIS AND CHARACTERISATION OF A NOVEL TYPE II B-RAF PARADOX BREAKER INHIBITOR

Rohit Arora, Joannes T.M. Linders, Samia Aci-Sèche, Thomas Verheyen,
Erika van Heerde, Dirk Brehmer, Apirat Chaikuad, Stefan Knapp, Pascal
Bonnet

► **To cite this version:**

Rohit Arora, Joannes T.M. Linders, Samia Aci-Sèche, Thomas Verheyen, Erika van Heerde, et al.. DESIGN, SYNTHESIS AND CHARACTERISATION OF A NOVEL TYPE II B-RAF PARADOX BREAKER INHIBITOR. European Journal of Medicinal Chemistry, 2023, 250, pp.115231. 10.1016/j.ejmech.2023.115231 . hal-04037562

HAL Id: hal-04037562

<https://hal.science/hal-04037562>

Submitted on 20 Mar 2023

HAL is a multi-disciplinary open access archive for the deposit and dissemination of scientific research documents, whether they are published or not. The documents may come from teaching and research institutions in France or abroad, or from public or private research centers.

L'archive ouverte pluridisciplinaire **HAL**, est destinée au dépôt et à la diffusion de documents scientifiques de niveau recherche, publiés ou non, émanant des établissements d'enseignement et de recherche français ou étrangers, des laboratoires publics ou privés.

1 **DESIGN, SYNTHESIS AND CHARACTERISATION OF A**
2 **NOVEL TYPE II B-RAF PARADOX BREAKER INHIBITOR**

3
4 Rohit Arora^{1,¶}, Joannes T.M. Linders², Samia Aci-Sèche¹, Thomas Verheyen², Erika Van Heerde², Dirk
5 Brehmer^{2,‡}, Apirat Chaikuad^{3,4}, Stefan Knapp^{3,4}, Pascal Bonnet¹

6
7 ¹ Institut de Chimie Organique et Analytique, UMR CNRS-Université d'Orléans 7311, Université
8 d'Orléans BP 6759, 45067 Orléans Cedex 2, France

9 ² Janssen Research and Development, a division of Janssen Pharmaceutica N.V., Turnhoutseweg 30,
10 Beerse 2340, Belgium

11 ³ Structural Genomics Consortium, Buchmann Institute for Life Science (BMLS), Max von Lauestrasse
12 15, 60438 Frankfurt am Main, Germany.

13 ⁴ Goethe-University, Institute for Pharmaceutical Chemistry, Max-von Laue Str. 9, 60438 Frankfurt am
14 Main, Germany.

15 [¶] Present address: Iktos Inc., 50 Milk St 16th Fl, Boston, MA 02109, USA

16 [‡] Present address: Dr. Falk Pharma GmbH, Leinenweberstraße 5, 79108 Freiburg im Breisgau,
17 Germany.

18
19
20
21

22

23

24

25

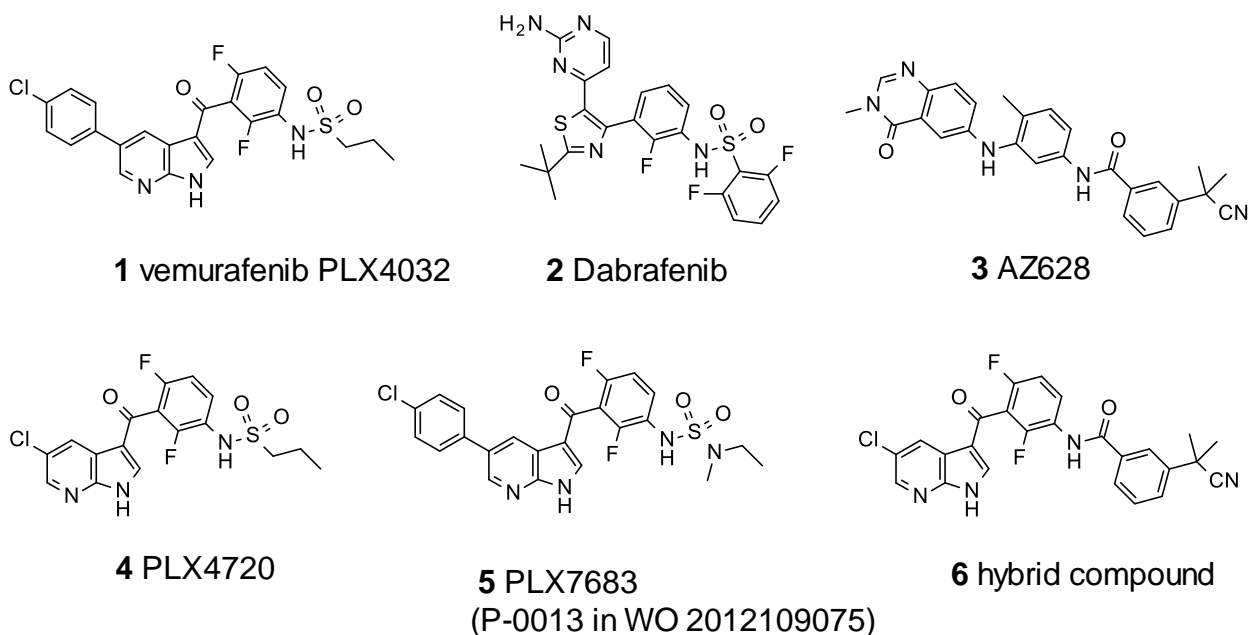
26

27 **ABSTRACT**

28 The mutation V600E in B-Raf leads to MAPK pathway activation, uncontrolled cell proliferation,
29 and tumorigenesis. ATP competitive type I B-Raf inhibitors, such as vemurafenib (**1**) and
30 PLX4720 (**4**) efficiently block the MAPK pathways in B-Raf mutant cells, however these
31 inhibitors induce conformational changes in the wild type B-Raf (^{wt}B-Raf) kinase domain leading
32 to heterodimerisation with C-Raf, causing paradoxical hyperactivation of the MAPK pathway.
33 This unwanted activation may be avoided by another class of inhibitors (type II) which bind the
34 kinase in the DFG-out conformation, such as AZ628 (**3**) preventing heterodimerization. Here
35 we present a new B-Raf kinase domain inhibitor that represents a *hybrid* between **4** and **3**. This
36 novel inhibitor borrows the hinge binding region from **4** and the back pocket binding moiety from
37 **3**. We designed, synthesized, determined its binding mode, performed activity/selectivity
38 studies, and molecular dynamics simulations in order to study the conformational effects
39 induced by this inhibitor on wt and V600E mutant B-Raf kinase. We discovered that the inhibitor
40 binds in a DFG-out/ α C-helix-in conformation, did not induce the aforementioned paradoxical
41 hyperactivation in the MAPK pathway, and it was active and highly selective for B-Raf. We
42 propose that this merging approach can be used to design a novel class of B-Raf inhibitors for
43 translational studies.

44 INTRODUCTION

45 Protein Kinases (PK) constitute the third largest protein families in eukaryotes and are
46 responsible for regulating most cellular signaling processes. Aberrant expression of PKs has
47 often been linked to cancer development, making PKs interesting targets for drug discovery
48 and development, and consequently, as of 2020, 68 small-molecule PK inhibitors (PKI) have
49 been approved by the FDA (Bournez et al., 2020; Ferguson and Gray, 2018; Roskoski, 2019).
50 B-Raf, a serine/threonine PK, is an important component of the RAS/Raf/MEK/ERK signal
51 transduction pathway (mitogen-activated protein kinase or MAPK signaling cascade) and it is
52 a key regulator of cell proliferation and survival (Robinson and Cobb, 1997). Binding of small
53 GTPases of the RAS family to B-Raf induce structural changes that trigger activation of B-Raf
54 and the MAPK signaling cascade which involves MEK kinases and ERK that phosphorylate
55 diverse substrates including transcription factors (Kolch, 2000; Morrison and Cutler, 1997). The
56 B-Raf V600E missense mutation is one of the most commonly observed mutations in
57 melanoma (Fiskus and Mitsiades, 2016; Holderfield et al., 2014). B-Raf V600E causes B-Raf
58 to signal independently from its upstream signaling partners leading to activation of MAPK
59 signaling resulting in increased cell proliferation and tumorigenesis (Cope et al., 2019; Davies
60 et al., 2002). Potent B-Raf inhibitors such as vemurafenib (Zelboraf®; **1** in Chart 1) (Bollag et
61 al., 2010) and dabrafenib (Tafinlar®; **2** in Chart 1) (Rheault et al., 2013) are highly effective for
62 treatment of patients with metastatic melanoma harboring the B-Raf V600E mutation (Carles
63 et al, 2018).



64
65 **Chart 1.** Known B-Raf inhibitors discussed in this paper.
66

67 However, the therapeutic effects of these inhibitors are challenged by rapid development of
68 drug resistance, and occurrence of secondary tumors such as cutaneous squamous cell
69 carcinoma and keratoacanthoma (Alcalá and Flaherty, 2012; Anforth et al., 2013; Solit and
70 Rosen, 2014). By targeting and stabilizing the active conformation of the wild-type B-Raf (^{wt}B-
71 Raf), these drugs paradoxically activate MAPK pathway giving rise to tumor development in
72 healthy tissue. Hence, these ATP-competitive inhibitors can either inhibit or (paradoxically)
73 activate the MAPK pathway depending on whether V600E mutant or ^{wt}B-Raf, is predominantly
74 expressed (Carnahan et al., 2010; Hatzivassiliou et al., 2010; Poulikakos et al., 2010). In fact,
75 this paradoxical activation was already reported in 1999 (Hall-Jackson et al., 1999).

76 During the past few years, this paradoxical activation of MAPK pathway by ATP-competitive B-
77 Raf inhibitors (paradox inducers; PI) has presented a novel and compelling challenge for
78 second generation B-Raf inhibitor development. Several mechanistic explanations have been
79 put forward to explain this phenomenon. A few recent studies have allowed drawing a consistent
80 picture of ^{wt}B-Raf inhibition by type I and II inhibitors targeting the active and inactive states of

81 the protein respectively, and subsequent events such as dimerization and MEK/ERK signaling
82 (paradoxical activation) (Peng et al., 2015; Yao et al., 2015; Zhang et al., 2015). In addition to
83 B-Raf homodimers, the B-Raf/C-Raf heterodimers may also act as paradoxical MAPK
84 activators (Heidorn et al., 2010) and both **1** and **2** (Chart 1) are weak inhibitors of C-Raf in
85 comparison to B-Raf. Therefore, it is unlikely that B-Raf/C-Raf heterodimers are effectively
86 inhibited by these drugs. Other studies have characterized the inhibitor binding mode and
87 monomer/dimer occupancy preference of many type II B-Raf inhibitors (for example BGB659,
88 AZ628, TAK-632, and BI882370), using their crystal structures in complex with B-Raf or B-
89 Raf/C-Raf heterodimer, to gain useful insights into the mechanism of inhibition and the
90 paradoxical activation (Liu and Gray, 2006, Yao et al. 2016, Hatzivassiliou et al., 2010, Wang
91 and Kim, 2012, Nakamura et al., 2013; Okaniwa et al., 2013, Lavoie et al., 2013, Waizenegger
92 et al., 2016).

93
94 In 2015, Zhang *et al.* (Zhang et al., 2015) reported the so-called 'paradox breaker' (PB)
95 compounds which intriguingly are structurally very close to **1**. Importantly these inhibitors were
96 not type II inhibitors, but they still did not cause paradoxical activation (Le et al., 2013; Zhang
97 et al., 2015). Briefly, the sulfonamide side chain present in the structure of **1**, was replaced by
98 an N-methyl,N-ethylsulfonylurea. Surprisingly, the crystal structures of the two complexes were
99 perfectly aligned, although there seemed to be some very subtle changes in the position of
100 Leu505, a residue positioned near the C-terminus of the α C-helix, which is an integral part of
101 the regulatory spine (R-spine) (Taylor and Kornev, 2011). Interestingly, when the 2,6-difluoro-
102 phenylsulfonamide in dabrafenib (**2**) was replaced by an N-methyl,N-ethylsulfonylurea tail, the
103 resulting compound showed reduced ERK activation, providing a new, rational basis for the
104 design of paradox breakers. In a follow up study, the same group (Yao et al., 2019)
105 demonstrated that the clinical candidate, PLX8394, only occupies one of the dimer active sites,

106 and disrupts B-Raf homo- and B-Raf-C-Raf heterodimers by very subtle interactions with
107 Leu505.

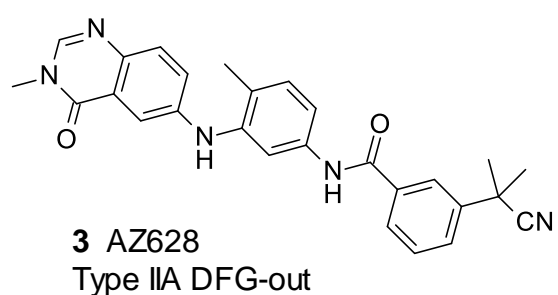
108 In 2017, a novel selective pan-Raf inhibitor REDX05358 was reported by Redx Pharma (Mason
109 et al., 2017), which, in comparison to vemurafenib, led to a more sustained inhibition of the
110 MAPK pathway. It was reported to induce minimal paradoxical activation in ^{wt}B-Raf cells by
111 inhibiting the MAPK signaling in both monomer and dimers with equal potencies. The crystal
112 structure for this compound is not yet available and therefore the structural features contributing
113 to paradox breaker properties are not known. In another recent study, Wang et al. (Wang et al.,
114 2017) have reported a new type II inhibitor designed by fragment linking method which has low
115 toxicity and is highly selective and active for B-Raf V600E. However, in the absence of the
116 crystal structure, it is difficult to ascertain the details of the binding mode. As of last year, next-
117 generation (dubbed as type IV) allosteric peptide B-Raf inhibitors have been introduced that
118 target the Raf dimerization interface, and in combination with ATP-competitive inhibitors also
119 prevent the paradoxical activation of the MAPK pathway (Beneker et al., 2019; Gunderwala et
120 al., 2019). For a relatively recent review of B-Raf inhibitors, see Agianian and Gavathiotis, 2018
121 (Agianian and Gavathiotis, 2018).

122 We analyzed four B-Raf kinase inhibitors, two paradoxical inducers (vemurafenib **1** and
123 PLX4720 **4**; Chart 1) and two paradox breakers (P-0013 (**5**; Chart 1) and P-0012 (Ibrahim et
124 al., 2009), to unravel the biological mechanism of inhibition of these compounds at a structural
125 and cellular level (Arora et al., 2015; Di Michele et al., 2015). From these studies, we identified
126 key structural features, in particular hydrogen bridges formed between gatekeeper T529
127 residue and the sulfonamide in **1** and **4**, which we hypothesized could combined with other
128 structural effects contribute to the paradoxical activation effect.

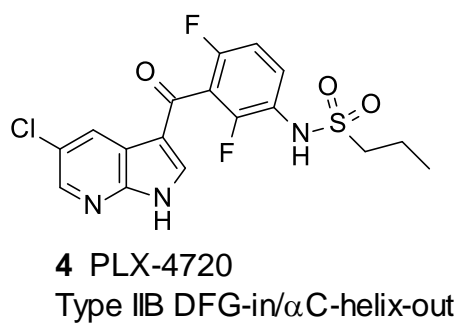
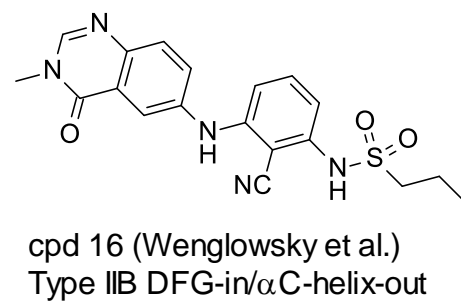
129 As part of our ongoing study of the B-Raf system, and to further contribute to the intense interest
130 in this field of research (Man et al., 2019; Wang et al., 2019; Yaeger and Corcoran, 2019,

131 Brummer and McInnes, 2020, Riegel and Rajalingam, 2020), here we focus on the design of
132 new paradoxical breaker inhibitor using structural information of both a type I and II kinase
133 inhibitors. We compared two inhibitors of B-Raf: **3** (type II DFG-out or type IIA DFG-out/ α C-
134 helix in) and **4** (classified as type I since it binds in the DFG-in conformation or as type IIB since
135 the α C-helix is in an “out” conformation). Previously, Wenglow sky *et al.* (Karoulia *et al.*, 2016;
136 Wenglow sky *et al.*, 2012, 2014) have shown that introduction of the sulfonamide side chain in
137 **3** changes the type II into a type I mode of binding in the B-Raf ATP active site. In order to keep
138 the physicochemical properties and 3-dimensional shape of the new hybrid compound similar
139 to **3**, we kept the 5-chloro-azaindole hinge region scaffold as present in **4** and the benzamide
140 side chain in **3** binding in the allosteric hydrophobic pocket (Scheme 1). With the substituted
141 azaindole moiety in place, we were able to draw conclusions about the importance of the
142 replacement of the propylsulfonamide by a substituted benzamide for the selection of type I or
143 type II binding modes.

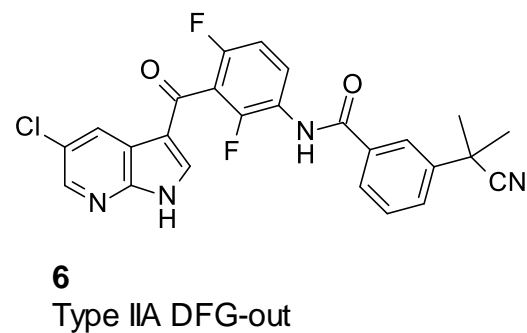
144 **Scheme 1.** Hybrids **16** and **6** from **3** and **4**
145



Wenglowsky et al
→



This work
→

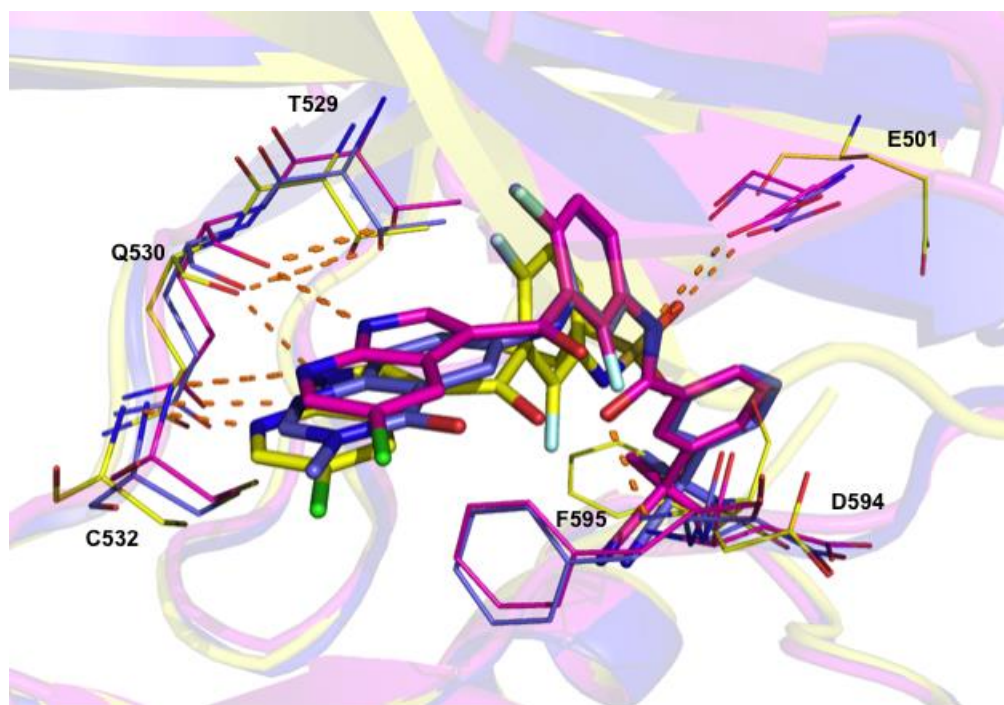


146
147

148

149 The superposition of the two crystal structures of **4** (PDB ID 3C4C) and **3** (PDB ID 4G9R) in B-
150 Raf highlighted the conserved structural elements present in the complex of the hybrid
151 compound **6** (Figure 1).

152 **Figure 1.** Superimposition of the B-Raf crystal structures of **3** (blue), **4** (yellow), **6** (magenta,
153 WT). Note the difference in the orientation of F595 for the DFG-in and DFG-out conformations
154



155
156
157

158 The interactions of the carboxylic acid group of Glu501, and the backbone NH of Asp594 with
159 the inhibitor potentially explain the selection of the type II folding. Docking studies of the hybrid
160 compound **6** with B-Raf were conducted in order to support our design hypothesis. Furthermore,
161 the synthesized B-Raf inhibitors were tested on a large panel of protein kinases to evaluate
162 their selectivity profile and were subsequently studied on two relevant human cell lines to
163 assess their paradoxical activation effects. Finally, the crystal structures of the hybrid compound
164 **6** in ^{wt}B-Raf and V600E mutant revealed a dimeric structure in which both ATP binding sites
165 were occupied.

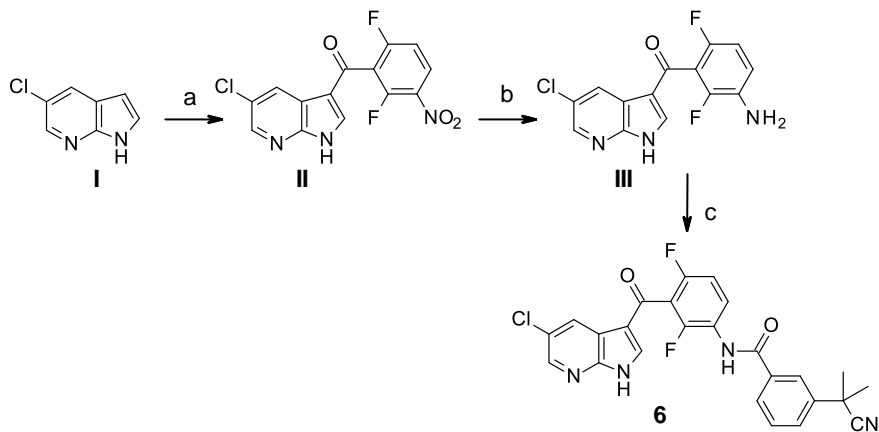
166

167 **RESULTS AND DISCUSSION**

168 **Synthesis of hybrid compound 6**

169 Hybrid compound **6** was prepared according to the scheme below (Scheme 2), which was
170 modified from the original synthesis of **4** (Tsai et al, 2008).

171 **Scheme 2.** A. 2,6-difluoro-3-nitro-benzoylchloride, AlCl₃, CH₂Cl₂, reflux, 96h, Y 50%; b. H₂,
172 Pt/C-5%, thiophene, THF, rt, 72 h, Y 96%; c. 3-dimethylacetone nitril-benzoylchloride, pyridine,
173 THF, rt, 16 h, 51%.
174



175

176 Briefly, Friedel-Crafts acylation of 5-chloro-1H-pyrrolo[2,3-b]pyridine **1** with benzoylchloride **II**
 177 gave keto derivative **III** in 50% yield after HPLC purification. Hydrogenation of the nitro group
 178 gave aniline **IV** in 96% yield, which was selectively acylated under standard conditions in 51%
 179 yield.

180 Hybrid compound **6** was tested in the ScanMAX kinase assay panel from Eurofins Discovery,
 181 together with **1**, **3-5**, and identified as a very potent inhibitor of both ^wB-Raf and B-Raf(V600E),
 182 but it was less selective than **3** and **4** (Table 1).

183

184 **Activity and selectivity of 1, 3, 4, 5 and 6 (ScanMAX)**

185 **Table 1.** Selected B-Raf inhibitors (Chart 1) with activity and selectivity data included

Compound	B-Raf IC ₅₀ [μM]	B-Raf(V600E) IC ₅₀ [μM]	Selectivity @1 μM (#kinase >50% inhibition/# kinase tested)	Other notable actives >80% inhibition@1 μM
1 (Vemurafenib)	0.130	0.062	30/451; 14/103	MEK5, PDGFRB, MEK4, KIT, FGR, Raf1
3 (AZ628)	0.0013	0.00085	28/103	PDGFRB, KIT, ABL1-nonphos., LCK, CSF1R, p38-α, RET, RSK1, CSK, p38-β, FLT1, BLK, FLT4, VEGFR2, PDGFRA, LYN, Raf1, HCK, SRC,

				YES, MEK5, TXK, FYN
4 (PLX4720)	0.025	0.037	19/103	MEK5, PDGFR, MEK4, Raf1, KIT, FGR
5 PLX7683 (P- 0013)	0.69	1.41	22/103	MEK5, VRK2, PDGFRB, BLK, FGR
6	0.056	0.048	38/103	KIT, BLK, CSF1R, FLT4, RET, MEK5, LCK, SRC, p38- α , MAP4K4, FLT3, FLT1, LYN, VEGFR2, FGR, p38- β , HCK, PDGFRA, TXK, FYN, Raf1, YES, ABL1-phos., FGFR2, CDK11, FGFR1, BMX, CSK

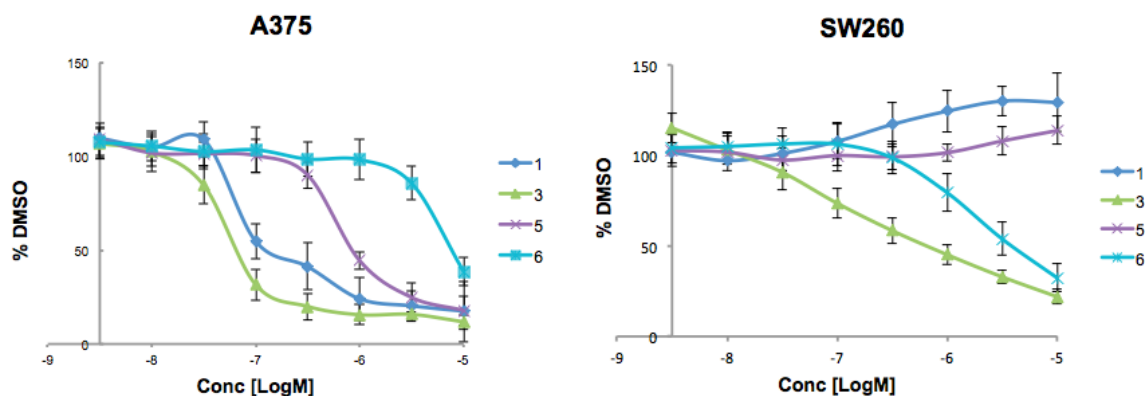
186

187 **Cell Viability and Downstream signaling**

188 In order to investigate the effect of the B-Raf inhibitors in living cells, the human colon cancer
189 cell line SW260 expressing ^{wt}B-Raf and the malignant melanoma A375 cell line expressing B-
190 Raf(V600E) were treated with increasing concentrations of B-Raf inhibitors. The MTT assays
191 (Figure 2; Table 2) showed that in the cell lines expressing B-Raf(V600E) all studied inhibitors

192 resulted in inhibition of proliferation, with varying potencies, the hybrid compound **6** being only
 193 weakly active. In SW260 expressing ^{wt}B-Raf, we observed a slight increase in proliferation at
 194 high concentration of **1** and **5**, but clear cytotoxicity of **3**, and the hybrid compound **6**. **1** and **5**
 195 show little toxicity in this cell line.

196 **Figure 2.** Treatment of malignant melanoma A375 cell line expressing B-Raf(V600E) (left
 197 panel); and human colon cancer cell line SW260 (^{wt}B-Raf; right panel) in MTT assay, by
 198 increasing concentrations of inhibitors **1**, **3**, **5** and **6**
 199



200
201

202

203 **Table 2:** Cytotoxicity as measured with an MTT assay for 4 selected compounds

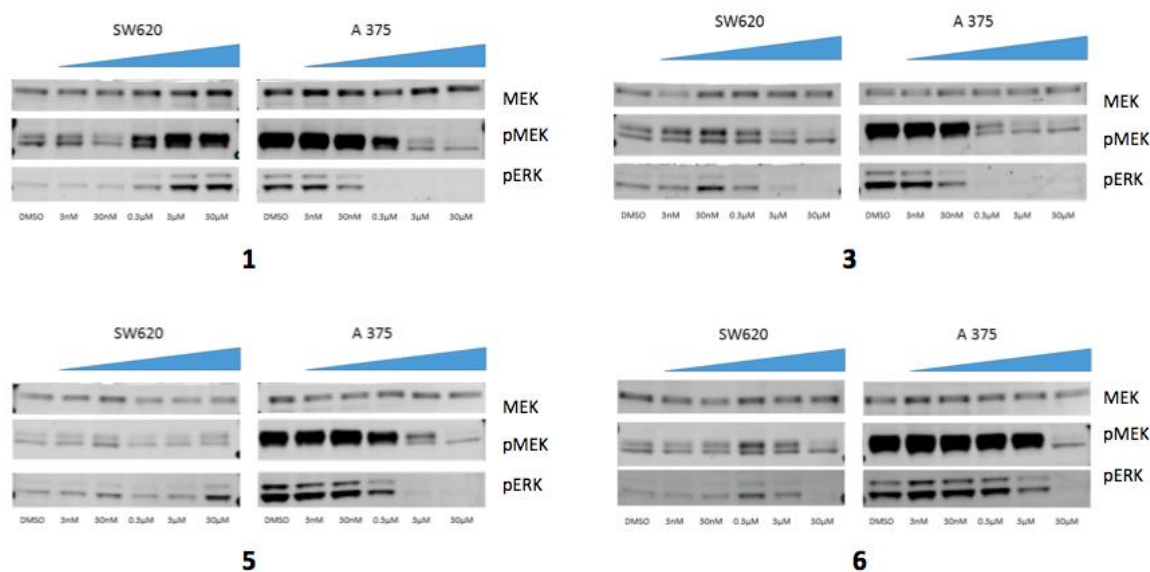
Compound	IC ₅₀ (μM)	
	SW620	A375
1	No inhibition, slight activation	0.088
3	0.166 μM	0.042
5	No inhibition, slight activation	0.560
6	2.810 μM	~10

204

205 The effect of the four B-Raf inhibitors on the MAPK signaling pathway was evaluated by
 206 measuring the phosphorylation of MEK and ERK. As expected, the treatment with all inhibitors
 207 led to reduced pMEK and pERK levels in cells expressing B-Raf(V600E) (Figures 2, 3). In cells

208 expressing ^{wt}B-Raf, **1** induced the pMEK and pERK levels due to paradoxical activation effects
209 (Figures 2, 3) in agreement with the previous reports (Zhang et al., 2015). As expected, paradox
210 breakers **3** and hybrid compound **6** showed little or no activation of ERK.

211 **Figure 3.** Western blot analyses of SW260 (expressing ^{wt}B-Raf) and A375 (expressing B-
212 Raf(V600E)) cell-lines treated with the inhibitors studied in this work. Treatment with **3** and
213 hybrid compound **6** does not lead to paradoxical ERK activation
214



215
216

217

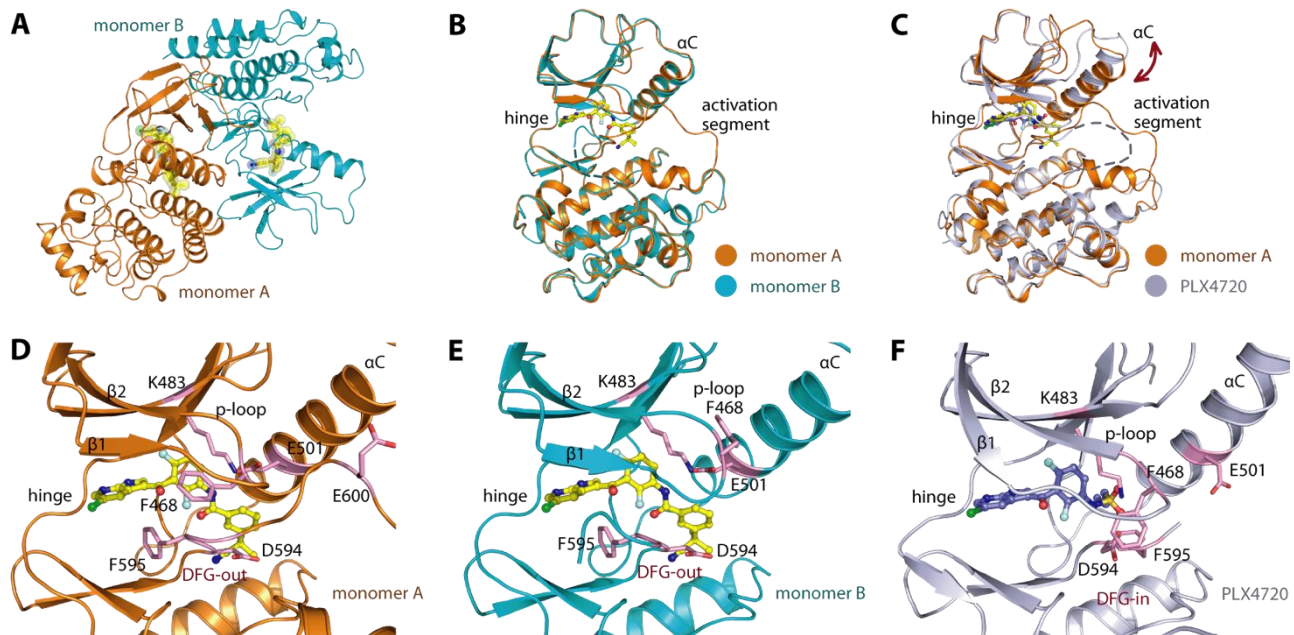
218 **Binding modes of 6 in wild type and V600E B-Raf**

219 From earlier studies by Wenglowsky *et al.* (Wenglowsky et al., 2011), it is known that the propyl-
220 and phenyl sulfonamide derivatives both bind to a DFG-in conformation with concomitant
221 movement of the α C-helix. In case of the phenylsulfonamides, a reorientation of Phe596, part
222 of DFG motif, is observed (PDB ID 3SKC). It is clear that the change from amide to sulfonamide
223 has a deciding impact on the binding mode. The amide in **3** is engaged in the canonical
224 hydrogen bond network with the backbone of Asp654 and the carboxylic acid of Glu501. To get
225 insight into the binding mode of hybrid compound **6** we co-crystallized this inhibitor with wild
226 type and V600E mutant B-Raf. The crystal structures showed a dimeric assembly with both
227 ATP sites occupied by the inhibitor in agreement with the lack of MAPK activation observed in

228 cellular assays. Dimeric structures are frequently observed even for inhibitors that break B-Raf
229 dimer in cellular assays due to the high protein concentration used in crystallization experiments
230 (Thevakumaran et al., 2015).

231 Superimposition of both monomers of the dimer revealed DFG-out (type-II) binding mode in
232 wild type as well as V600E mutant B-Raf (Figure 4). We observed however a number of striking
233 structural features by comparing the monomer structures. α C-helix was in an “in” position as
234 indicated by formation of the canonical salt bridge between the VAIK motif lysine (K483) and
235 the α C glutamate (E501).

236 **Figure 4.** Structure of B-Raf in complex with **6**. A) dimeric B-Raf in the crystal structure. B)
237 Superimposition of the two monomers demonstrating different state of the activation segment,
238 which is fully ordered in monomer A but disordered in B. C) Structural comparison with **4**
239 reveals not only distinct DFG conformations, ‘out’ in this structure, and ‘in’ in **4** (pdb code
240 3C4C), but also slight difference in the α C-helix positions. Close-up details of the inhibitor
241 binding sites in monomer A and B with **6** (D and E, respectively) and **4** (F).
242



243
244
245

246 Despite the induced DFG-out conformation, the activation segment was well organized in chain
247 A of the monomer but was unstructured in chain B, this might be due to crystal contacts. In the
248 mutant, E600 was involved in a number of long-range polar interactions with the α C N-terminus

249 (Q493) but the residue was too distant to form efficient hydrogen bonds. In chain B the
250 activation segment was oriented towards the solvent and it was unstructured after residue T599.
251 The DFG phenylalanine (F595) stacked end on against the aromatic ring system of the
252 pyrrolopyridine hinge binding motif which formed the expected ATP mimetic hydrogen bonds
253 with the main chain carbonyl of Q530 and the amid nitrogen with C532. Differences were seen
254 between the interactions of the P-loop phenylalanine (F468) with the inhibitor. In chain A, the
255 P-loop phenylalanine was flipped into the active site causing a strong distortion of the P-loop
256 and the phenylalanine side chain was stabilized by aromatic stacking interaction with the
257 inhibitor. In chain B the P-loop F468 was extended in an active conformation interacting with
258 α C-helix. A similar P-loop conformation has been described for **4** (PDB ID: 3C4C). However, **4**
259 assumes a type I binding mode stabilizing a displaced α C-helix that rotated around its axis
260 removing the conserved α C glutamate (E501) from the ATP site.

261 The sulfonamide in **4**, a paradox inducer complexed in the DFG-in form of B-Raf, was engaged
262 in hydrogen bond with the backbone of Phe595 and Gly596 and potentially with the side-chain
263 of Lys483, as observed in the PDB structure 3C4C but not in the PDB structure 4WO5. These
264 changes in the hydrogen bond network are accompanied by a switch of the α C-helix from the
265 “in” state to the “out” state. A similar behavior has been observed for **1**, for which the
266 sulfonamide motif is linked to the main chain of Phe595 and Gly596 with an α C-helix-out
267 conformation. When replacing the sulfonamide motif by an amide in the hybrid compound **6**,
268 the canonical hydrogen bond network described previously was restored, causing the α C-helix
269 to assume an “in” conformation. However, based on the α C-helix conformations of other
270 inhibitors (Table 3), it is unlikely that the conformation of the α C-helix alone explained the
271 paradoxical breaker effect of **3** and of our hybrid inhibitor. Indeed, we notice in Table 3, listing
272 the X-ray structures of B-Raf complexes, 3 PB inhibitors (PLX7904, PLX7922 and BI 882370)
273 induced an α C-helix-out conformation in B-Raf. On the other hand, the B-Raf structures

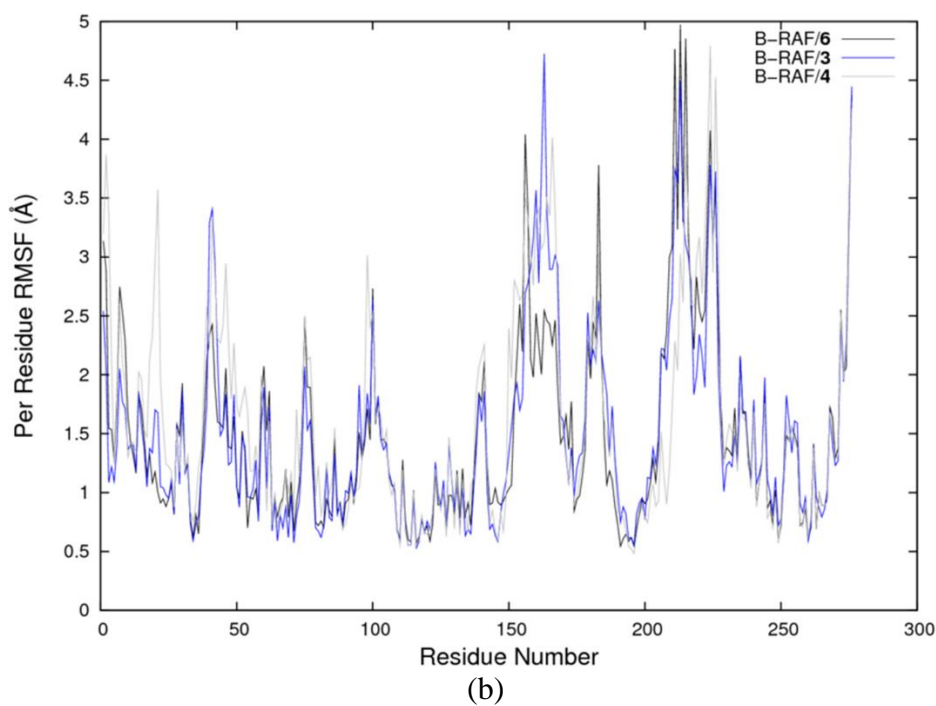
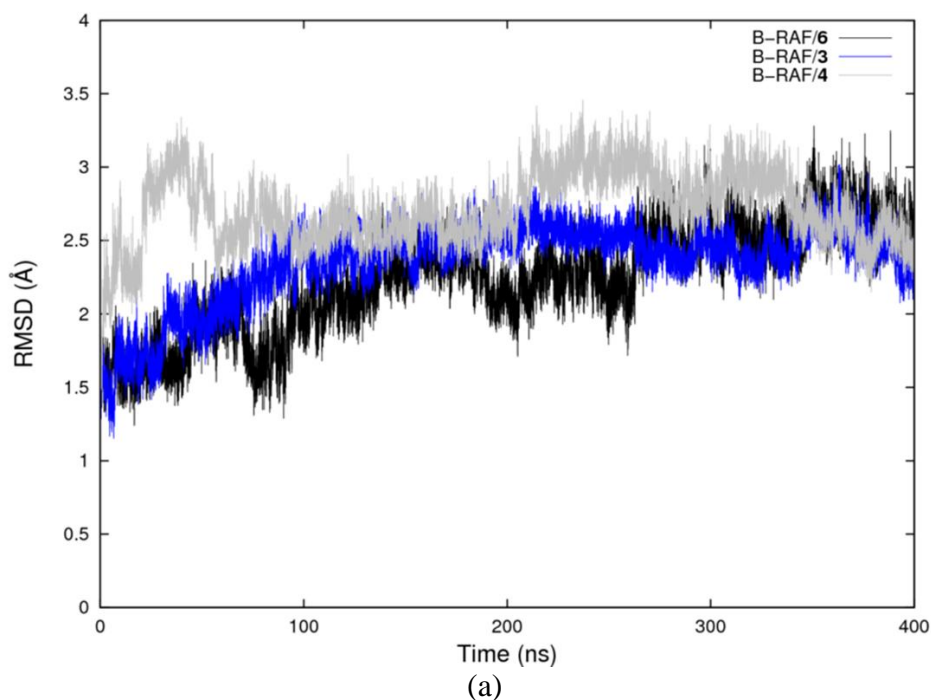
274 complexed with paradox inducer compounds may have an α C-helix with “in” or “out”
275 conformation. One conclusion that emerged from structural information of B-Raf inhibitor
276 complexes listed in Table 3 was that if the ligand harbors a sulfonamide or a sulfonyl urea motif,
277 the α C-helix adopts an “out” conformation, regardless of whether the ligand is a paradox
278 breaker or paradox inducer and whether the inhibitor induces DFG-in or a DFG-out
279 conformation. Therefore, we studied the conformational dynamics of B-Raf in complex with
280 these inhibitors using molecular dynamics (MD) simulations.

281

282 **MD simulations of the human ^{wi}B-Raf inhibitor complexes**

283 400 ns of MD simulations were carried out on the three inhibitor complexes: B-Raf/**3**, B-Raf/**4**
284 and B-Raf/**6**. The α C-helix RMSDs (Figure 5(a)) showed that each of the three simulations
285 reached equilibrium around a RMSD of 2.5 Å with respect to their respective experimental
286 structures. The per-residue RMSF profiles for the B-Raf kinase domain complexed with each
287 of the three ligands are shown in Figure 5(b).

288 **Figure 5.** (a) Root Mean Squared Deviation (RMSD); and (b) Per residue Root Mean
289 Squared Fluctuation (RMSF) during 400ns of MD simulation of B-Raf complexed with **3**, **4** and
290 **6**

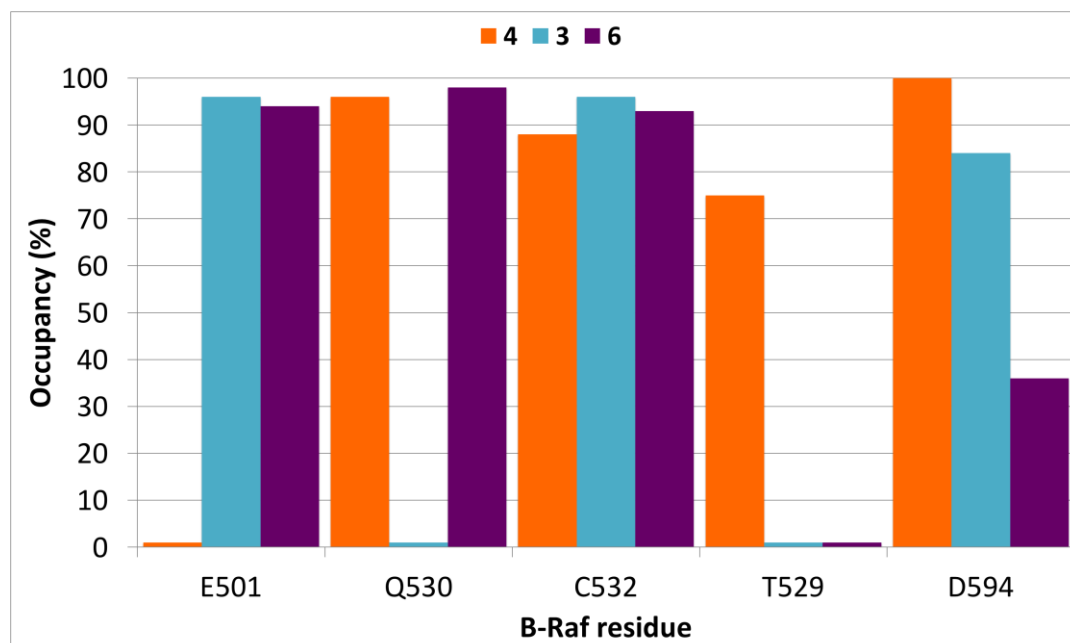


297 We observed that the RMSF profiles for the B-Raf kinase domain complexed with **3** and with **6**
 298 were very similar. In comparison, the B-Raf kinase domain complexed with **4** was observed to
 299 be slightly more flexible than the two other systems, with a $\langle \text{RMSF} \rangle = 0.61 \text{ \AA}$ for B-Raf/4
 300 compared to a $\langle \text{RMSF} \rangle = 0.49 \text{ \AA}$ for B-Raf/3 and B-Raf/6. The hydrogen bond network between

301 the ligand and the receptor was analysed for each system. The analyses of these data are
302 summarized in Figure 6. The H-bonds with the hinge residues, C532 for AZ628, Q530, and
303 C532 for PLX4720 and the hybrid compound, were retained throughout the simulations. We
304 observe an additional H-bond with E501 for the two PB compounds which probably stabilizes
305 an “in” conformation of the α C-helix. We have previously reported interaction between type I PI
306 inhibitors **1** and **4**, and the gatekeeper residue T529 of B-Raf wild type over 100 ns MD
307 simulation, whereas this interaction was not observed with type I PB inhibitors (such as **5**)
308 (Arora et al. 2015).

309 **Figure 6.** Bar chart showing the hydrogen bond occupancy between the analyzed inhibitors
310 and important B-Raf residues, including the gatekeeper residue T529

311

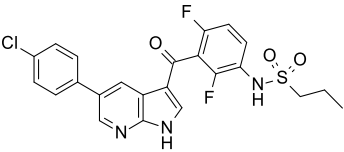
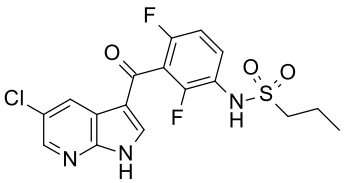


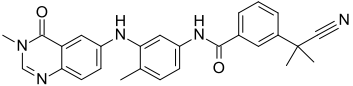
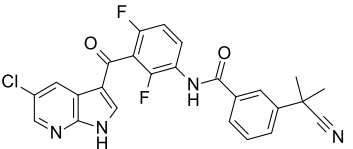
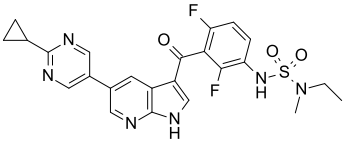
312
313

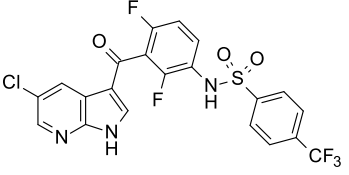
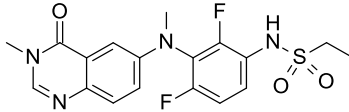
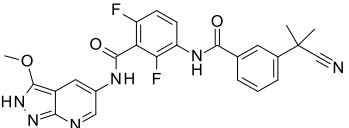
314 In the current work, we also observe the interaction between T529 and **4** complexed with ^{wt}B-
315 Raf over 400 ns MD simulations. It is noteworthy that this interaction with the gatekeeper
316 residue was not observed in the two crystal structures of ^{wt}B-Raf complexed with **1** and **4**,
317 respectively PDB ID 3OG7 and PDB ID 3C4C. It appeared that this interaction could be one of

318 the features that could be discriminatory between type I paradoxical inducer (PI) and breaker
319 (PB) inhibitors, although the structural and conformational basis of such discrimination is not
320 clear. However, this argument may be strengthened by the observation that during our MD
321 simulations this interaction was also absent in ^wtB-Raf complexed with **3**, a PB inhibitor which
322 binds type IIB binding mode. Consequently, we expected, and indeed observed, that **6**, another
323 PB inhibitor binding in type IIB binding mode, did not exhibit this interaction (Figure 6).

324 **Table 3** Comparison of binding modes of compounds discussed in this paper

Compound	Binding mode	PI or PB	PDB	Remark	Ref.	Chain A			Chain B		
						DFG (d _F -HRD Å)	αC (d _{E-K} Å) side chains (d _{E-K} Å) Cα-Cα	occupied	DFG (d _F -HRD Å)	αC-helix (d _{E-K} Å) side chains (d _{E-K} Å) Cα-Cα	occupied
Vemurafenib (1) 	IIB	PI	3OG7	V600E	(Bollag et al., 2010)	in (4.8)	out (8.4) (13.4)	yes	in (5.2)	in (2.6) (11.6)	no
PLX4720 (4) 	IIB	PI	3C4C	WT	(Tsai et al., 2008)	in (5.2)	out (8.7) (13.6)	yes	out (10.6)	in (7.1) (12.1)	yes
			4WO5	WT	(Thevakumaran et al., 2015)	in	out	yes	in	Out	yes

						(5.9)	(10.9)		(5.6)	(~11.9)	
							(13.9)			(14.1)	
AZ628 (3) 	IIA	PB	4G9R	V600E	(Wenglowsky et al., 2012)	out (10.3)	in (3.5) (11.3)	yes	out (10.4)	In (3.4) (11.3)	yes
Our hybrid (6) 	IIA	PB	To be submitted	WT	This work	out (10.3)	in (2.865) (11.038)	yes	out (10.4)	in (2.726) (11.070)	yes
			To be submitted	V600E	This work	out (10.3)	in (2.976) (10.929)	yes	out (10.4)	in (2.775) (10.995)	yes
PLX7904 	IIB	PB	4XV1	V600E X-ray alternative for P-0013 (PLX7683)	(Zhang et al., 2015)	in (4.7)	out (8.082) (13.245)	yes	in (5.6)	in (4.117) (11.499)	no

PLX5568 	IIA	PI	4XV9	WT	(Zhang et al., 2015)	out (10.7)	in/out? (8.750) (13.326)	yes	N/A	N/A	N/A
Compound 18/2VX 	IIB	N/A	4PP7	WT X-ray alternative for cpd16	(Wenglowsky et al., 2014)	in (4.8)	out (11.715) (13.701)	yes	in (4.8)	out (11.215) (13.510)	yes
Compound 4/0WP 	IIA	N/A	4G9C	WT	(Wenglowsky et al., 2012)	out (10.3)	in (3.0) (11.1)	yes	out (10.3)	in (3.0) (11.1)	yes
Dabrafenib	IIB	PI	4XV2	V600E	(Zhang et al., 2015)	in (4.2)	out (7.5) (12.6)	yes	in (4.4)	in (9.7) (12.3)	yes
			5CSW	WT	(Waizenegger et al., 2016)	in	out	yes	in	out	yes

						(4.3)	(7.4) (12.6)		(4.5)	(8.7) (12.9)	
---	--	--	--	--	--	-------	-----------------	--	-------	-----------------	--

325

326 **Discussion**

327 In 2017, Wang *et al.* reported a series of pyrimidine scaffolds as potent pan-Raf inhibitors
328 containing a benzamide functionality that engaged Glu501 and Asp594 in a hydrogen
329 bonding network in a DFG-out orientation (Wang *et al.*, 2017). The hybrid B-Raf inhibitor
330 studied and characterized here utilized a similar scaffold and was observed to adopt a
331 DFG-out conformation.

332 Many ATP-competitive B-Raf inhibitors have been shown to induce dimerization of the
333 BRAF kinase domains, where the protomer units are placed side-to-side and the dimer
334 interface located near the α C-helix (Hu *et al.*, 2013; Rajakulendran *et al.*, 2009). It has
335 previously been shown that the relative position of α C-helix, as induced by the inhibitor,
336 is a factor in determining the occupancy of each protomer. For instance, a B-Raf inhibitor
337 such as TAK632, which stabilizes the α C-helix in “in” conformation, allows for the second
338 protomer to be also occupied by an inhibitor molecule (Nakamura *et al.*, 2013; Okaniwa
339 *et al.*, 2013). In comparison, **1** stabilizes the α C-helix in “out” conformation and does not
340 allow for the other protomer in the B-Raf dimer to be occupied by an inhibitor molecule
341 (as seen in chain B of crystal structure 3OG7) (Karoulia *et al.*, 2016). Recent molecular
342 dynamics studies have suggested that an inter-protomer interaction of a dimer mediated
343 via the conserved N-terminal W450 residue (in B-Raf) resulting in a direct interaction of
344 the two R-spine motifs. Therefore, any dimer conformational change would likely involve
345 a disruption of this interaction of R-spines (Jambrina *et al.*, 2016). At the level of paradox
346 inducer and paradox breaker inhibitors, it has been suggested that the paradox inducer
347 inhibitors promote dimer-formation more than paradox breaker inhibitors, which leads to
348 enhanced activation. Essentially, paradox inducer inhibitors may hinder the

349 conformational changes, which may disrupt the dimer assembly, in the α C-helix region
350 (Kondo et al., 2019; Tsai and Nussinov, 2018; Tse and Verkhivker, 2016), as has also
351 been noted by Jambrina *et al.* This further emphasizes the role of the conformational
352 changes in the Raf dimer interface in paradoxical activation of the MAPK pathway
353 introduced by ATP-competitive inhibitors. However, a type II B-Raf inhibitor such as
354 AZ628 (**3**) also strongly introduces Raf-dimerisation, but does not trigger the paradoxical
355 activation characteristically caused by inhibitor-induced dimerisation (notably with type I
356 inhibitors as discussed above), as has been noted in the literature (Noeparast et al., 2018;
357 Savoia et al., 2019; Wang and Kim, 2012) and has been confirmed by the current study.
358 This is attributed to sterically allowing occupancy of both protomers of the Raf dimer by **3**
359 due to its longer residence time. This mechanism is consistent with that of another type II
360 pan-Raf inhibitor TAK-632. The crystal structure of **6** with B-Raf dimer also revealed
361 occupancy in both protomers (Figure 7). Owing to the similarity in structures and binding
362 modes of **6** and **3**, this suggests a similar mechanism of inhibitor-induced dimerization
363 and therefore a function of **6** as paradoxical breaker inhibitor. Binding of the hybrid
364 compound is essentially identical into WT and mutant protein.

365

366

367 Given the important role of the conformation of the α C-helix in Raf activation and
368 dimerization, more recent structural hypotheses about the involved residues are worth
369 noting, specifically the role of the residue R506 which has been deemed to be crucial. It
370 has been hypothesized that the orientation of the R506 residue alone can affect the B-

371 Raf dimerization. It has also been reported that in the third generation PB inhibitors (such
372 as PLX7904, PLX8934) the orientation of R506 is “out” along with rest of the α C-helix
373 which prevents these inhibitors from promoting paradoxical activation (Karoulia et al.,
374 2016). The orientation of R506 in some second generation (paradox inducer) B-Raf
375 inhibitors such as vemurafenib (**1**) and dabrafenib is “in”. The orientation of this residue
376 R506 in our hybrid B-Raf (WT)/**6** has also been observed to be “out” which further points
377 to a structural interpretation of its PB nature.

378

379 **SIGNIFICANCE**

380 The discovery of B-Raf inhibitor **6** represents a novel approach to design effective hybrid
381 B-Raf inhibitors, which utilise the features of both type I and type II B-Raf inhibitors and
382 do not paradoxically activate the MAPK pathway. This may represent a new class of
383 inhibitors altogether and can help in enhancing our existing knowledge of mechanisms
384 involved in B-Raf activation by inhibitors.

385

386 **EXPERIMENTAL PROCEDURES**

387

388 **Preparation of B-Raf complex models**

389 The crystal structure of the human ^{wt}B-Raf kinase domain (KD) complexed with the hybrid
390 compound has been mutated at multiple sites in order to improve expression to allow
391 crystallization. The starting B-Raf KD model was prepared using the Homology Modeling
392 software Modeller 9.13 (Sali and Blundell, 1993). The sequence of the B-Raf KD was

393 obtained from its UniProt entry (B-Raf_HUMAN, P15056, isoform 1). The crystal structure
394 of the B-Raf KD complexed with the hybrid compound was used as a template for building
395 the B-Raf KD model. This structure is in a DFG-out/ α C-helix-out conformation. The co-
396 crystallized ligand in the template-binding site and the interacting water molecules were
397 constraint for induced fit for the generation of five models. The same protocol was used
398 for the generation of initial models for the human ^{wt}B-Raf KD complexed with AZ628 and
399 PLX4720. The crystal structures used as template for the building of these two other
400 models were the structure with PDB ID 4G9R and 3C4C respectively.

401

402 **Molecular Dynamics Simulations**

403 Molecular dynamics (MD) simulations were carried out on the B-Raf-inhibitor complex
404 models that were obtained as described in the previous section. All simulations were
405 carried out using the Amber14 suite (Case et al., 2014) with the Amber12SB force field
406 parameters. The parameter and coordinate files for the inhibitors were prepared using the
407 antechamber utility (Wang et al., 2006) of AmberTools14. GAFF force field parameters
408 (Wang et al., 2004) were used for the inhibitors, and the partial charges were calculated
409 using the AM1-BCC method. The topology files for the protein–inhibitor complexes were
410 prepared using the tleap utility of AmberTools14. All the systems were then solvated using
411 a TIP3P solvent box of 10 Å radii from protein surface counter-ions were added to
412 neutralize the system reaching a ionic strength of 0.15 M. In order to remove any possible
413 structural artifacts resulting from model building, before running the MD simulations, the
414 solvated systems were subjected to minimization. This was performed in three steps. In
415 the first step, positional restraints on the position of the solute molecules were applied,

416 and only the solvent and ion molecules were allowed to minimize for 100 steps using the
417 steepest descent method followed by 2000 steps using the conjugate gradient method.
418 In the second step, positional restraints were applied on the atoms of the solvent
419 molecules leaving the solute molecule free to minimize during 100 steps using steepest
420 descent algorithm followed by 2000 steps using the gradient conjugate methods. In the
421 third step, the entire system was subjected to minimization for 100 steps using the
422 steepest descent method followed by 2000 steps using the conjugate gradient method.
423 Following the minimization step, the systems were heated from 0 to 300 K using a
424 Langevin thermostat, at a constant volume, for 20 ps with time step of 2 fs. A weak
425 restraint of 10 kcal/(mol·Å²) was applied on the solute during this run. Once the system
426 was heated to 300 K, the solute restraints were gradually removed during 10 ps at a
427 constant volume, and the systems were then equilibrated over a period of 400 ps with a
428 time step of 2 fs under constant pressure conditions in order to relax the solvent density.
429 Finally, the production runs were carried out using the NPT ensemble for 400 ns with a
430 nonbonded cut off of 10 Å and time steps of 2 fs at 300 K. During the equilibration and
431 production steps, bonds involving hydrogens were constrained using the SHAKE
432 algorithm. Long range electrostatic interactions were treated using the particle mesh
433 Ewald (PME) method (Walker et al., 2008). All the simulations were carried out using the
434 PMEMD module of the Amber14 suite, which is the reimplementation of Sander utility,
435 with improved performance on a GPU cluster.

436 **Chemistry**

437 Detailed experimental procedures can be found in the Supplementary material.

438

439

440 **Crystallography**

441 **Crystallography and structure analysis**

442 Recombinant ^{wt}B-Raf and B-Raf(V600E), both harboring 16 surface mutations, were
443 expressed and purified as described previously (Thevakumaran et al., 2015; Tsai et al.,
444 2008). Purified proteins in 20 mM HEPES, pH 7.5, 150 mM NaCl, 1 mM TCEP and 5%
445 glycerol at 10-12 mg/ml were mixed with **6** at 2.5-fold molar excess, and the complexes
446 were crystallized using sitting drop vapour diffusion method at 20 °C and various
447 conditions as summarized in the table 4. Diffraction data collected at Diamond Light
448 Source, beamline I03 using wavelength of 0.97624 Å were processed and scaled with
449 Mosflm (Powell et al., 2013) and Scala, (Evans, 2006) respectively. Molecular
450 replacement was performed using Phaser (McCoy et al., 2007)
451 and the coordinates of published B-Raf structure (Thevakumaran et al., 2015). Iterative
452 cycles of model rebuilding alternated with structure refinement were performed in COOT
453 (Emsley et al., 2010) and REFMAC (Murshudov et al., 2011) respectively. The final
454 models were verified for their geometric correctness using MolProbity (Chen et al., 2010) .
455 The data collection and refinement statistics are summarized in the table 4.

456 **Table 4:** Description of the final crystallographic models

Complex	^{wt}B-Raf/6	B-Raf(V600E)/6
PDB accession code	XXXX	XXXX
<i>Data Collection</i>		
Resolution ^a (Å)	57.45-1.65	74.55-1.65

	(1.74-1.65)	(1.74-1.65)
Spacegroup	$P2_12_12_1$	$P2_12_12_1$
Cell dimensions	$a = 49.1, b = 97.6, c = 114.9 \text{ \AA}$	$a = 49.3, b = 97.7, c = 115.3 \text{ \AA}$
	$\alpha = \gamma = \beta = 90.0^\circ$	$\alpha = \gamma = \beta = 90.0^\circ$
No. unique reflections ^a	66,629 (9,169)	67,419 (9,443)
Completeness ^a (%)	99.1 (95.2)	99.4 (97.3)
$I/\sigma I^a$	21.2 (9.4)	19.3 (6.4)
R_{merge}^a (%)	0.066 (0.166)	0.067 (0.245)
Redundancy ^a	8.4 (6.8)	8.1 (6.5)
Refinement		
No. atoms in refinement (P/L/O) ^b	4,345/68/574	4,306/68/574
B factor (P/L/O) ^b (\AA^2)	17/11/27	17/11/29
R_{fact} (%)	15.4	15.2
R_{free} (%)	17.1	17.5
rms deviation bond ^c (\AA)	0.016	0.016
rms deviation angle ^c ($^\circ$)	1.6	1.6
Molprobit Ramachandran		
Favour (%)	96.79	97.16
Outlier (%)	0	0
Crystallization conditions	19% PEG3350, 0.1M	13% PEG3350, 0.2M

	bis-tris-propane pH 7.0, 0.2M sodium bromide, 10% ethylene glycol	sodium nitrate, 5% ethylene glycol
--	---	---------------------------------------

457 ^a Values in brackets show the statistics for the highest resolution shells.

458 ^b P/L/O indicate protein, ligand molecules presented in the active sites, and other (water
459 and solvent molecules), respectively.

460 ^c rms indicates root-mean-square.

461

462 **Activity Assays**

463 Cell Viability

464 SW620 and A375 cells were obtained from ATCC. Cell viability assays (MTT) were carried
465 out as described by Mosmann (Mosmann 1983). In brief, cells were seeded at 4000 and
466 1000 per well (96 well format), respectively, and treated with compounds the next day for
467 96 h. The compounds' impact on cell viability was analysed via the MTT assay.

468

469 Immunoblotting

470 SW620 and A375 cells were seeded at 750 000 and 300 000 cells per well (six well format)
471 and 48 h later (75% confluence) treated with increasing compound concentrations for
472 either 1 or 4 h. Cells were lysed in lysis buffer (10 mM Tris-HCL, 1% SDS, and 20 mM
473 Na₃VO₄) and 10–25 µg of proteins from each sample were loaded, separated by SDS-
474 PAGE, and transferred to PVDF membranes. Membranes were incubated with the
475 indicated primary antibodies and analyzed by the Odyssey detection system from LI-COR.

476 Used primary antibodies for MEK, phospho-MEK, and phospho-ERK were purchased
477 from Cell Signaling, B-Raf from Santa Cruz, and actin from Sigma. Corresponding
478 secondary antibodies were used from Rockland and Invitrogen.

479

480

481 **ACCESSION NUMBERS**

482 The Protein Data Bank accession number for the hybrid compound **5**-bound to ^{wt}B-Raf
483 and V600E mutant structures reported in this paper is **XXXX** and **XXXX** respectively.

484

485

486 **ACKNOWLEDGEMENTS**

487 This work was supported by a research project grant (IWT 110431) from the Institute for
488 the Promotion of Innovation by Science and Technology in Flanders (IWT) to DB. RA and
489 PB are grateful to Janssen Pharmaceutica for financial support. We gratefully
490 acknowledge the CaSciModOT Centre de Calcul Scientifique de la Région Centre Val de
491 Loire for providing computer facilities. AC and SK are grateful for support by the SGC, a
492 registered charity that receives funds from; AbbVie, Bayer AG, Boehringer Ingelheim,
493 Canada Foundation for Innovation, Eshelman Institute for Innovation, Genentech,
494 Genome Canada through Ontario Genomics Institute [OGI-196],
495 EU/EFPIA/OICR/McGill/KTH, Diamond Innovative Medicines Initiative 2 Joint
496 Undertaking [EUbOPEN grant 875510], Janssen, Merck KGaA (aka EMD in Canada and
497 US), Merck & Co (aka MSD outside Canada and US), Pfizer, São Paulo Research
498 Foundation-FAPESP, Takeda and Wellcome. AC and SK would also like to acknowledge

499 support by the Frankfurt Cancer Centre (FCI and the German translational cancer
500 network (DKTK).

501

502 REFERENCES

Agianian, B., and Gavathiotis, E. (2018). Current Insights of BRAF Inhibitors in Cancer. *J. Med. Chem.* *61*, 5775–5793.

Alcalá, A.M., and Flaherty, K.T. (2012). BRAF inhibitors for the treatment of metastatic melanoma: clinical trials and mechanisms of resistance. *Clin. Cancer Res.* *18*, 33–39.

Anforth, R., Fernandez-Peñas, P., and Long, G.V. (2013). Cutaneous toxicities of RAF inhibitors. *Lancet Oncol.* *14*, e11-18.

Arora, R., Di Michele, M., Stes, E., Vandermarliere, E., Martens, L., Gevaert, K., Van Heerde, E., Linders, J.T.M., Brehmer, D., Jacoby, E., et al. (2015). Structural investigation of B-Raf paradox breaker and inducer inhibitors. *J. Med. Chem.* *58*, 1818–1831.

Beneker, C.M., Rovoli, M., Kontopidis, G., Röring, M., Galda, S., Braun, S., Brummer, T., and McInnes, C. (2019). Design and Synthesis of Type-IV Inhibitors of BRAF Kinase That Block Dimerization and Overcome Paradoxical MEK/ERK Activation. *J. Med. Chem.* *62*, 3886–3897.

Bollag, G., Hirth, P., Tsai, J., Zhang, J., Ibrahim, P.N., Cho, H., Spevak, W., Zhang, C., Zhang, Y., Habets, G., et al. (2010). Clinical efficacy of a RAF inhibitor needs broad target blockade in BRAF-mutant melanoma. *Nature* *467*, 596–599.

Bournez, C., Carles, F., Peyrat, G., Aci-Sèche, S., Bourg, S., Meyer, C., & Bonnet, P. (2020). Comparative Assessment of Protein Kinase Inhibitors in Public Databases and in PKIDB. *Molecules* *25*, 3226.

Brummer, T., & McInnes, C. (2020). RAF kinase dimerization: implications for drug discovery and clinical outcomes. *Oncogene*, 1-15.

Carles, F., Bourg, S., Meyer, C., and Bonnet, P. (2018). PKIDB: A Curated, Annotated and Updated Database of Protein Kinase Inhibitors in Clinical Trials. *Molecules* *23*, 908.

Carnahan, J., Beltran, P.J., Babij, C., Le, Q., Rose, M.J., Vonderfecht, S., Kim, J.L., Smith, A.L., Nagapudi, K., Broome, M.A., et al. (2010). Selective and potent Raf inhibitors paradoxically stimulate normal cell proliferation and tumor growth. *Mol. Cancer Ther.* *9*, 2399–2410.

Case, D.A., Babin, V., Berryman, J., Betz, R.M., Cai, Q., Cerutti, D.S., Cheatham III, T.E., Darden, T.A., Duke, R.E., Gohlke, H., et al. (2014). Amber 14.

Chen, V.B., Arendall, W.B., Headd, J.J., Keedy, D.A., Immormino, R.M., Kapral, G.J., Murray, L.W., Richardson, J.S., and Richardson, D.C. (2010). MolProbity: all-atom structure validation for macromolecular crystallography. *Acta Crystallogr. D Biol. Crystallogr.* *66*, 12–21.

Cope, N., Novak, B., Candelora, C., Wong, K., Cavallo, M., Gunderwala, A., Liu, Z., Li, Y., and Wang, Z. (2019). Biochemical Characterization of Full-Length Oncogenic BRAFV600E together with Molecular Dynamics Simulations Provide Insight into the Activation and Inhibition Mechanisms of RAF Kinases. *ChemBioChem* 20, 2850–2861.

Davies, H., Bignell, G.R., Cox, C., Stephens, P., Edkins, S., Clegg, S., Teague, J., Woffendin, H., Garnett, M.J., Bottomley, W., et al. (2002). Mutations of the BRAF gene in human cancer. *Nature* 417, 949–954.

Di Michele, M., Stes, E., Vandermarliere, E., Arora, R., Astorga-Wells, J., Vandebussche, J., van Heerde, E., Zubarev, R., Bonnet, P., Linders, J.T.M., et al. (2015). Limited Proteolysis Combined with Stable Isotope Labeling Reveals Conformational Changes in Protein (Pseudo)kinases upon Binding Small Molecules. *J. Proteome Res.* 14, 4179–4193.

Emsley, P., Lohkamp, B., Scott, W.G., and Cowtan, K. (2010). Features and development of Coot. *Acta Crystallogr. D Biol. Crystallogr.* 66, 486–501.

Evans, P. (2006). Scaling and assessment of data quality. *Acta Crystallogr. D Biol. Crystallogr.* 62, 72–82.

Ferguson, F.M., and Gray, N.S. (2018). Kinase inhibitors: the road ahead. *Nat Rev Drug Discov* 17, 353–377.

Fiskus, W., and Mitsiades, N. (2016). B-Raf Inhibition in the Clinic: Present and Future. *Annu. Rev. Med.* 67, 29–43.

Gunderwala, A.Y., Nimbvikar, A.A., Cope, N.J., Li, Z., and Wang, Z. (2019). Development of Allosteric BRAF Peptide Inhibitors Targeting the Dimer Interface of BRAF. *ACS Chem. Biol.* 14, 1471–1480.

Hall-Jackson, C.A., Evers, P.A., Cohen, P., Goedert, M., Boyle, F.T., Hewitt, N., Plant, H., and Hedge, P. (1999). Paradoxical activation of Raf by a novel Raf inhibitor. *Chem. Biol.* 6, 559–568.

Hatzivassiliou, G., Song, K., Yen, I., Brandhuber, B.J., Anderson, D.J., Alvarado, R., Ludlam, M.J.C., Stokoe, D., Gloor, S.L., Vigers, G., et al. (2010). RAF inhibitors prime wild-type RAF to activate the MAPK pathway and enhance growth. *Nature* 464, 431–435.

Heidorn, S.J., Milagre, C., Whittaker, S., Noury, A., Niculescu-Duvas, I., Dhomen, N., Hussain, J., Reis-Filho, J.S., Springer, C.J., Pritchard, C., et al. (2010). Kinase-dead BRAF and oncogenic RAS cooperate to drive tumor progression through CRAF. *Cell* 140, 209–221.

Holderfield, M., Deuker, M.M., McCormick, F., and McMahon, M. (2014). Targeting RAF kinases for cancer therapy: BRAF-mutated melanoma and beyond. *Nat. Rev. Cancer* 14, 455–467.

Hu, J., Stites, E.C., Yu, H., Germino, E.A., Meharena, H.S., Stork, P.J.S., Kornev, A.P., Taylor, S.S., and Shaw, A.S. (2013). Allosteric activation of functionally asymmetric RAF kinase dimers. *Cell* 154, 1036–1046.

Ibrahim, P.N., Spevak, W., Cho, H., and Shi, S. (2009). Compounds and methods for kinase modulation, and indications therefor.

Jambrina, P.G., Rauch, N., Pilkington, R., Rybakova, K., Nguyen, L.K., Kholodenko, B.N., Buchete, N.-V., Kolch, W., and Rosta, E. (2016). Phosphorylation of RAF Kinase Dimers Drives Conformational Changes that Facilitate Transactivation. *Angewandte Chemie International Edition* 55, 983–986.

Karoulia, Z., Wu, Y., Ahmed, T.A., Xin, Q., Bollard, J., Krepler, C., Wu, X., Zhang, C., Bollag, G., Herlyn, M., et al. (2016). An Integrated Model of RAF Inhibitor Action Predicts Inhibitor Activity against Oncogenic BRAF Signaling. *Cancer Cell* 30, 485–498.

Kolch, W. (2000). Meaningful relationships: the regulation of the Ras/Raf/MEK/ERK pathway by protein interactions. *Biochem. J.* 351 Pt 2, 289–305.

Kondo, Y., Ognjenović, J., Banerjee, S., Karandur, D., Merk, A., Kulhanek, K., Wong, K., Roose, J.P., Subramaniam, S., and Kuriyan, J. (2019). Cryo-EM structure of a dimeric B-Raf:14-3-3 complex reveals asymmetry in the active sites of B-Raf kinases. *Science* 366, 109–115.

Lavoie, H., Thevakumaran, N., Gavory, G., Li, J., Padeganeh, A., Guiral, S., Duchaine, J., Mao, D.Y.L., Bouvier, M., Sicheri, F., et al. (2013). Inhibitors that stabilize a closed RAF kinase domain conformation induce dimerization. *Nat Chem Biol* 9, 428–436.

Le, K., Blomain, E.S., Rodeck, U., and Aplin, A.E. (2013). Selective RAF inhibitor impairs ERK1/2 phosphorylation and growth in mutant NRAS, vemurafenib-resistant melanoma cells. *Pigment Cell Melanoma Res* 26, 509–517.

Liu, Y., and Gray, N.S. (2006). Rational design of inhibitors that bind to inactive kinase conformations. *Nat. Chem. Biol.* 2, 358–364.

Man, R.-J., Zhang, Y.-L., Jiang, A.-Q., and Zhu, H.-L. (2019). A patent review of RAF kinase inhibitors (2010–2018). *Expert Opinion on Therapeutic Patents* 29, 675–688.

Mason, H., Scrace, S., Testar, R., Rainard, J., Talab, F., Poonawala, R., Smith, P., Brooke, H., Frith, S., Ahmet, J., et al. (2017). Abstract 5160: Development of REDX05358, a novel highly selective and potent pan RAF inhibitor and a potential therapeutic for BRAF and RAS mutant tumors. *Cancer Res* 77, 5160–5160.

McCoy, A.J., Grosse-Kunstleve, R.W., Adams, P.D., Winn, M.D., Storoni, L.C., and Read, R.J. (2007). Phaser crystallographic software. *J Appl Crystallogr* 40, 658–674.

Morrison, D.K., and Cutler, R.E. (1997). The complexity of Raf-1 regulation. *Curr. Opin. Cell Biol.* 9, 174–179.

Mosmann, T. (1983). Rapid Colorimetric Assay for Cellular Growth and Survival: Application to Proliferation and Cytotoxicity Assays. *J. Immunol. Methods.* 65, 55–63.

Murshudov, G.N., Skubák, P., Lebedev, A.A., Pannu, N.S., Steiner, R.A., Nicholls, R.A., Winn, M.D., Long, F., and Vagin, A.A. (2011). REFMAC5 for the refinement of macromolecular crystal structures. *Acta Crystallogr. D Biol. Crystallogr.* 67, 355–367.

Nakamura, A., Arita, T., Tsuchiya, S., Donelan, J., Chouitar, J., Carideo, E., Galvin, K., Okaniwa, M., Ishikawa, T., and Yoshida, S. (2013). Antitumor activity of the selective pan-RAF inhibitor TAK-632 in BRAF inhibitor-resistant melanoma. *Cancer Res.* 73, 7043–7055.

Noeparast, A., Giron, P., De Brakeleer, S., Eggermont, C., De Ridder, U., Teugels, E., and De Grève, J. (2018). Type II RAF inhibitor causes superior ERK pathway

suppression compared to type I RAF inhibitor in cells expressing different BRAF mutant types recurrently found in lung cancer. *Oncotarget* 9, 16110–16123.

Okaniwa, M., Hirose, M., Arita, T., Yabuki, M., Nakamura, A., Takagi, T., Kawamoto, T., Uchiyama, N., Sumita, A., Tsutsumi, S., et al. (2013). Discovery of a selective kinase inhibitor (TAK-632) targeting pan-RAF inhibition: design, synthesis, and biological evaluation of C-7-substituted 1,3-benzothiazole derivatives. *J. Med. Chem.* 56, 6478–6494.

Peng, S.-B., Henry, J.R., Kaufman, M.D., Lu, W.-P., Smith, B.D., Vogeti, S., Rutkoski, T.J., Wise, S., Chun, L., Zhang, Y., et al. (2015a). Inhibition of RAF Isoforms and Active Dimers by LY3009120 Leads to Anti-tumor Activities in RAS or BRAF Mutant Cancers. *Cancer Cell* 28, 384–398.

Poulikakos, P.I., Zhang, C., Bollag, G., Shokat, K.M., and Rosen, N. (2010). RAF inhibitors transactivate RAF dimers and ERK signalling in cells with wild-type BRAF. *Nature* 464, 427–430.

Powell, H.R., Johnson, O., and Leslie, A.G.W. (2013). Autoindexing diffraction images with iMosflm. *Acta Cryst D* 69, 1195–1203.

Rajakulendran, T., Sahmi, M., Lefrançois, M., Sicheri, F., and Therrien, M. (2009). A dimerization-dependent mechanism drives RAF catalytic activation. *Nature* 461, 542–545.

Rheault, T.R., Stellwagen, J.C., Adjabeng, G.M., Hornberger, K.R., Petrov, K.G., Waterson, A.G., Dickerson, S.H., Mook, R.A., Laquerre, S.G., King, A.J., et al. (2013). Discovery of Dabrafenib: A Selective Inhibitor of Raf Kinases with Antitumor Activity against B-Raf-Driven Tumors. *ACS Med Chem Lett* 4, 358–362.

Riegel, K., & Rajalingam, K. (2020). The non-linearity of RAF-MEK signaling in dendritic cells. *Cell Cycle*, 1-11.

Robinson, M.J., and Cobb, M.H. (1997). Mitogen-activated protein kinase pathways. *Curr. Opin. Cell Biol.* 9, 180–186.

Roskoski, R. (2019). Properties of FDA-approved small molecule protein kinase inhibitors. *Pharmacological Research* 144, 19–50.

Sali, A., and Blundell, T.L. (1993). Comparative protein modelling by satisfaction of spatial restraints. *J. Mol. Biol.* 234, 779–815.

Savoia, P., Fava, P., Casoni, F., and Cremona, O. (2019). Targeting the ERK Signaling Pathway in Melanoma. *Int J Mol Sci* 20.

Solit, D.B., and Rosen, N. (2014). Towards a Unified Model of RAF Inhibitor Resistance. *Cancer Discov* 4, 27–30.

Taylor, S.S., and Kornev, A.P. (2011). Protein kinases: evolution of dynamic regulatory proteins. *Trends Biochem. Sci.* 36, 65–77.

Thevakumaran, N., Lavoie, H., Critton, D.A., Tebben, A., Marinier, A., Sicheri, F., and Therrien, M. (2015). Crystal structure of a BRAF kinase domain monomer explains basis for allosteric regulation. *Nat. Struct. Mol. Biol.* 22, 37–43.

- Tsai, C.-J., and Nussinov, R. (2018). Allosteric activation of RAF in the MAPK signaling pathway. *Current Opinion in Structural Biology* 53, 100–106.
- Tsai, J., Lee, J.T., Wang, W., Zhang, J., Cho, H., Mamo, S., Bremer, R., Gillette, S., Kong, J., Haass, N.K., et al. (2008). Discovery of a selective inhibitor of oncogenic B-Raf kinase with potent antimelanoma activity. *Proc. Natl. Acad. Sci. U.S.A.* 105, 3041–3046.
- Tse, A., and Verkhivker, G.M. (2016). Exploring Molecular Mechanisms of Paradoxical Activation in the BRAF Kinase Dimers: Atomistic Simulations of Conformational Dynamics and Modeling of Allosteric Communication Networks and Signaling Pathways. *PLoS ONE* 11, e0166583.
- Waizenegger, I.C., Baum, A., Steurer, S., Stadtmüller, H., Bader, G., Schaaf, O., Garin-Chesa, P., Schlattl, A., Schweifer, N., Haslinger, C., et al. (2016). A Novel RAF Kinase Inhibitor with DFG-Out-Binding Mode: High Efficacy in BRAF-Mutant Tumor Xenograft Models in the Absence of Normal Tissue Hyperproliferation. *Mol. Cancer Ther.* 15, 354–365.
- Walker, R.C., Crowley, M.F., and Case, D.A. (2008). The implementation of a fast and accurate QM/MM potential method in Amber. *J Comput Chem* 29, 1019–1031.
- Wang, X., and Kim, J. (2012). Conformation-Specific Effects of Raf Kinase Inhibitors. *J. Med. Chem.* 55, 7332–7341.
- Wang, J., Wolf, R.M., Caldwell, J.W., Kollman, P.A., and Case, D.A. (2004). Development and testing of a general amber force field. *Journal of Computational Chemistry* 25, 1157–1174.
- Wang, J., Wang, W., Kollman, P.A., and Case, D.A. (2006). Automatic atom type and bond type perception in molecular mechanical calculations. *Journal of Molecular Graphics and Modelling* 25, 247–260.
- Wang, L., Zhang, Q., Zhu, G., Zhang, Z., Zhi, Y., Zhang, L., Mao, T., Zhou, X., Chen, Y., Lu, T., et al. (2017). Design, synthesis and evaluation of derivatives based on pyrimidine scaffold as potent Pan-Raf inhibitors to overcome resistance. *Eur J Med Chem* 130, 86–106.
- Wang, P.-F., Qiu, H.-Y., and Zhu, H.-L. (2019). A patent review of BRAF inhibitors: 2013-2018. *Expert Opin Ther Pat* 29, 595–603.
- Wenglowsky, S., Ren, L., Ahrendt, K.A., Laird, E.R., Aliagas, I., Alicke, B., Buckmelter, A.J., Choo, E.F., Dinkel, V., Feng, B., et al. (2011). Pyrazolopyridine Inhibitors of B-Raf(V600E). Part 1: The Development of Selective, Orally Bioavailable, and Efficacious Inhibitors. *ACS Med Chem Lett* 2, 342–347.
- Wenglowsky, S., Moreno, D., Laird, E.R., Gloor, S.L., Ren, L., Risom, T., Rudolph, J., Sturgis, H.L., and Voegtli, W.C. (2012). Pyrazolopyridine inhibitors of B-Raf(V600E). Part 4: rational design and kinase selectivity profile of cell potent type II inhibitors. *Bioorg. Med. Chem. Lett.* 22, 6237–6241.
- Wenglowsky, S., Ren, L., Grina, J., Hansen, J.D., Laird, E.R., Moreno, D., Dinkel, V., Gloor, S.L., Hastings, G., Rana, S., et al. (2014). Highly potent and selective 3-N-

methylquinazoline-4(3H)-one based inhibitors of B-Raf(V600E) kinase. *Bioorg. Med. Chem. Lett.* **24**, 1923–1927.

Yaeger, R., and Corcoran, R.B. (2019). Targeting Alterations in the RAF–MEK Pathway. *Cancer Discov* **9**, 329–341.

Yao, H., Sun, Q., and Zhu, J. (2016). Identification and Characterization of Small-Molecule Inhibitors to Selectively Target the DFG-in over the DFG-out Conformation of the B-Raf Kinase V600E Mutant in Colorectal Cancer. *Arch. Pharm. (Weinheim)* **349**, 808–815.

Yao, Z., Torres, N.M., Tao, A., Gao, Y., Luo, L., Li, Q., de Stanchina, E., Abdel-Wahab, O., Solit, D.B., Poulikakos, P.I., et al. (2015). BRAF Mutants Evade ERK-Dependent Feedback by Different Mechanisms that Determine Their Sensitivity to Pharmacologic Inhibition. *Cancer Cell* **28**, 370–383.

Yao, Z., Gao, Y., Su, W., Yaeger, R., Tao, J., Na, N., Zhang, Y., Zhang, C., Rymar, A., Tao, A., et al. (2019). RAF inhibitor PLX8394 selectively disrupts BRAF dimers and RAS-independent BRAF-mutant-driven signaling. *Nat Med* **25**, 284–291.

Zhang, C., Spevak, W., Zhang, Y., Burton, E.A., Ma, Y., Habets, G., Zhang, J., Lin, J., Ewing, T., Matusow, B., et al. (2015). RAF inhibitors that evade paradoxical MAPK pathway activation. *Nature* **526**, 583–586.

503

504

505

506 **Supplementary materials**

507 **Chemistry**

508 **General**

509 ¹H NMR spectra were recorded with Bruker Avance DPX 400 and 360 spectrometers, and

510 chemical shifts (δ) are expressed in parts per million (ppm) with TMS as internal standard. For

511 all tested and final compounds where no analytical purity is mentioned, compounds were

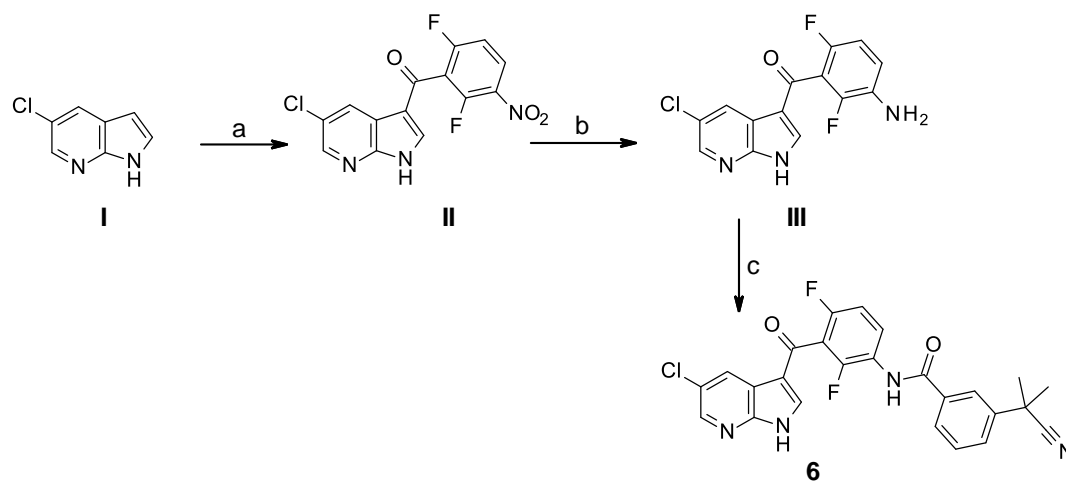
512 confirmed >95% pure via HPLC methods.

513 Compounds **1**, **3**, and **4** were obtained from SelleckChem, and compound **5** was synthesized

514 according to the procedure in WO 2012109075.

515

516 **Preparation of hybrid compound 6**

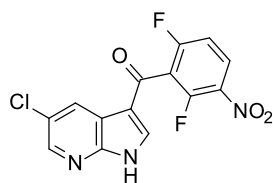


517

518 **2,6-Difluoro-3-nitro benzoyl chloride**

519 DMF (0.19 ml, 2.4 mmol) was added to a solution of 2,6-difluoro-3-nitro-benzoic acid (7.0 g,
520 34.5 mmol) in thionyl chloride (70 ml) at room temperature. The mixture was stirred and heated
521 to reflux overnight ($\pm 80^{\circ}\text{C}$; SOCl_2 $T_b=74.6^{\circ}\text{C}$). Excess of thionyl chloride was removed under
522 reduced pressure. 2,6-Difluoro-3-nitro benzoyl chloride was not isolated and directly used for the
523 next step.

524

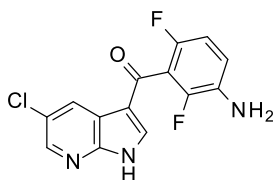


525

526 **(5-Chloro-1H-pyrrolo[2,3-b]pyridin-3-yl)-(2,6-difluoro-3-nitro-phenyl)methanone (II):**

527 Aluminum chloride (24.0 g, 180 mmol) was dissolved in DCM (105 ml) under an atmosphere of
528 nitrogen below 5°C . I (3.4 g, 22.4 mmol) in DCM (52.5 ml) was added and the reaction mixture
529 was stirred for 1 hour. 2,6-Difluoro-3-nitro benzoyl chloride (7.0 g, 31.6 mmol) in DCM (52.5

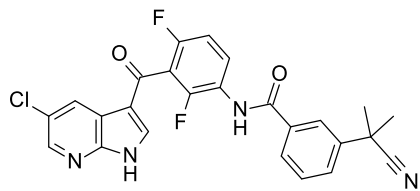
530 ml) was added at 0°C dropwise. The mixture was left stirring for six days at 45°C. After six days
531 the mixture was poured in aqueous HCl (1N) solution (300 ml) yielding compound **II** (4.83 g,
532 91%) as a white yellowish precipitate, which was used in the next step without further
533 purification. Additional **II** was isolated from the organic layer and further purified by Prep
534 HPLC (Stationary phase: RP Vydac Denali C18 - 10µm, 200g, 5cm, Mobile phase: 0.25%
535 NH₄HCO₃ solution in water, CH₃CN) yielding another fraction of **II** (480 mg) as a white
536 yellowish solid. ¹H NMR (360 MHz, DMSO-*d*₆) δ ppm 8.43 (s, 2 H), 8.18 (s, 1 H), 6.84 - 7.00
537 (m, 2 H), 5.24 (s, 2 H). MS (ESI) [M-H]⁻ = 335.99 and 335.92 found.



538
539 **(3-Amino-2,6-difluoro-phenyl)-(5-chloro-1H-pyrrolo[2,3-b]pyridin-3-yl)methanone (III):** To
540 **II** (1.0 g, 2.9 mmol) in THF (50 ml) was added Pt/C-5% (200 mg) and a 4% solution of
541 thiophene in diisopropyl ether (0.5 ml). Hydrogen was inserted in the reaction mixture and left
542 stirring for three days. The mixture was filtered over decalite and concentrated under reduced
543 pressure yielding **III** (923 mg, 93%) as a white yellowish powder. ¹H NMR (360 MHz, DMSO-
544 *d*₆) δ ppm 5.24 (s, 2 H) 6.82 - 7.04 (m, 2 H) 8.10 - 8.27 (m, 2 H) 8.43 (s, 2 H). MS (ESI) [M-H]⁻
545 = 306.02 and 305.92 found.

546

547



548

549 **N-[3-(5-chloro-1H-pyrrolo[2,3-b]pyridine-3-carbonyl)-2,4-difluoro-phenyl]-3-(1-cyano-1-**
550 **methyl-ethyl)benzamide (6)**

551 To a solution of **III** (0.20 g, 0.65 mmol) in anhydrous THF, pyridine (0.5 mL, 6.5 mmol) is
552 added, followed by 3-dimethylacetone nitril-benzoylchloride (0.15 g, 0.72 mmol). After stirring
553 overnight at room temperature under a nitrogen atmosphere, the reaction mixture is concentrated,
554 and the residue is purified by Prep HPLC (Stationary phase: Uptisphere C18 ODB - 10 μ m, 200g,
555 5cm), Mobile phase: 0.25% NH₄HCO₃ solution in water, CH₃CN) , yielding the title compound
556 (0.16 g, 0.33 mmol, 51% yield) as a solid white material.

557 ¹H NMR (360 MHz, DMSO-*d*₆) δ ppm 13.17 (br s, 1 H), 10.41 (s, 1 H), 8.49 (d, *J*=2.4 Hz, 1 H),
558 8.46 (d, *J*=2.4 Hz, 1 H), 8.26 (s, 1 H), 8.11 (t, *J*=1.8 Hz, 1 H), 7.97 (d, *J*=7.7 Hz, 1 H), 7.75 -
559 7.85 (m, 2 H), 7.62 (t, *J*=7.8 Hz, 1 H), 7.35 (t, *J*=8.8 Hz, 1 H), 1.75 (s, 6 H) MS (ESI) [M-H]⁻ =
560 306.02 and 305.92 found.

561

562